Journal of the Australian Ceramic Society (2022) 58:287–298
https://doi.org/10.1007/s41779-021-00689-9

RESEARCH

The ion irradiation tolerance of the fluorite RE_2MO_5 (RE = Sm, and Yb, M = Ti, Zr, and Sn) system

Robert D. Aughterson[1] · Robin Newman[2] · Mihail Ionescu[1] · Gregory R. Lumpkin[1]

Received: 1 August 2021 / Revised: 16 November 2021 / Accepted: 25 November 2021 / Published online: 6 December 2021

Abstract

In the search for novel ceramics for use within nuclear fuel–related applications and nuclear waste-form matrices, a major focus has been on the development of radiation-tolerant materials. Of particular interest in this field have been numerous compounds with either pyrochlore or the related fluorite-type structures. In this study, we look to expand the family of compounds with defect fluorite–type structure. We have fabricated three new compounds; $Yb_2Sn_{1.125}O_{5.25}$, $Yb_2Sn_{1.25}O_{5.5}$, and $Yb_2Sn_{1.375}O_{5.75}$. The compound $Yb_2Sn_{1.125}O_{5.25}$ was determined, via x-ray diffraction, to have the long-range defect fluorite structure, *Fm*-3 *m* symmetry, with cell parameter $a = 5.17233(1)$. Further to this, Sm_2ZrO_5 and Yb_2TiO_5 compounds were also fabricated and crystal structures characterised. The use of transmission electron microscopy has revealed a much more complex crystal structure than that of the relatively high symmetry fluorite, with the presence of structural modulations being detected. The ion-irradiation response of these compounds was tested via bulk specimen irradiation using 15-MeV gold ions with grazing incidence x-ray diffraction characterisation. The results show that both Sm_2ZrO_5 and $Yb_2Sn_{1.25}O_{5.5}$ are highly tolerant to ion-irradiation exposure whilst Yb_2TiO_5 is susceptible to amorphisation.

Keywords Pyrochlore · Fluorite · Ion-irradiation · Nuclear ceramics

Introduction

Rare earth (RE) metal oxides, in particular pyrochlores and fluorites, have been the subject of much ongoing interest in both nuclear and electrochemical research. These ceramics have desirable properties including high flux and fluence radiation tolerance [1–3], whilst some also have high ionic conductivity [4–6]. By using stoichiometries of the form $RE_2M_xO_{3+2x}$ ($1 \leq x \leq 2$), where RE^{3+} is a rare earth, and M^{4+} a smaller metal cation, pyrochlore through to defect fluorite structures may be fabricated within these solid solutions. However, solid solutions can only be achieved for certain combinations of rare earth and metal cations [7, 8].

For the rare earth titanate compounds of RE_2TiO_5 stoichiometry, a variety of structures and chemistries exist. A range of applications for these compounds have been studied including burnable poisons [9, 10], containment matrices for immobilisation of high-level nuclear waste [11–16], lithium ion and sodium ion batteries [17], and electronic and ionic conductivity [18–20]. Application-based studies on RE_2ZrO_5 and RE_2SnO_5 compositions are almost non-existent although there has been some interest in the zirconates for nuclear-based use, e.g. inert matrix–type fuels with poisons [8].

Via experimental observation of the $RE_2M_2O_7$ system of compounds, it has been empirically shown that the ionic radius ratios between RE and metal cations (r_{RE}/r_M) influence which crystal structure type will form [6]. For specific cation radius ratios, the closely related cubic fluorites ($r_{RE}/r_M < 1.46$) and pyrochlores ($r_{RE}/r_M = 1.46$ to 1.78) form. For the RE_2TiO_5 system, the empirically derived cation ratio phase stability regions no longer apply, and other crystal structure types and polymorphs are available depending on fabrication conditions and cation radii ratios, including orthorhombic and hexagonal symmetry [21]. For the combinations of cations of the $RE_2M_2O_7$ stoichiometry (RE = rare earths, and M = Ti, Sn, and Zr), the stability fields are dominated by either pyrochlore or fluorite structure with only a

✉ Robert D. Aughterson
roa@ansto.gov.au

[1] Institute of Materials Engineering, Australian Nuclear Science and Technology Organisation, Lucas Heights, NSW 2234, Australia

[2] Intellectual Property Office, Concept House Cardiff Road, Newport NP108QQ, South Wales, UK

few titanates, La to $Nd_2Ti_2O_7$ having either the $P2_1$ or $Cmc2_1$ space groups. For the RE_2MO_5 system, there is a stability field for either pyrochlore or fluorite structure for the lanthanide titanates from Dy to Lu_2TiO_5; this is broader for the lanthanide zirconates Pr to Lu_2ZrO_5 [8] and for the stannates is limited to the slightly off-stoichiometry $Yb_2Sn_{1+x}O_{5+2\times}$ investigated in this study.

The structural difference achieved in the transition between fluorite (MO_2), defect fluorite (MO_{2-x}), and pyrochlore ($RE_2M_2O_7$) is slight, involving the removal of oxygen from the (8a) anion site, changing of the *48f* oxygen *x* positional parameter from 0.3125 (ideal pyrochlore) to 0.375 (ideal fluorite), and ordering of the cations onto separate A and B sites. RE_2MO_5 fits onto the pyrochlore lattice in the style $RE_2(RE_{0.33}M_{0.67})_2O_{6.67}$ where there is some mixing of the two cations on the B-site and increased anion vacancies relative to the ideal pyrochlore $RE_2M_2O_7$ stoichiometry. Alternatively, for the defect-fluorite structure, there will be disorder over the RE and M-sites, also with further increased anion vacancies ($MO_{1.67}$).

There are limited solid solutions when looking at the RE_2MO_5 to $RE_2M_2O_7$ (RE = rare-earths, M = Ti, Zr, Sn, and Hf) systems [8]. For the titanates, solid solutions exist for rare earths from terbium to lutetium with all being described as pyrochlore-type structure, *Fd*-3 *m* symmetry [22]. However, in further studies, several RE_2TiO_5 (RE = Dy, Ho, Er, and Yb) compounds have been described as long-range defect fluorite with nano-domains of pyrochlore-type structure [10, 23–25]. There are complete solid solutions for most rare earth zirconates and hafnates [7] with multi-phase, 2 or more crystal structure types, regions mainly occurring for the larger rare earths; La_2ZrO_5 (pyrochlore plus cubic phases), La_2HfO_5 (pyrochlore plus hexagonal phases), Pr_2HfO_5 (pyrochlore plus fluorite phases), and Nd_2HfO_5 (pyrochlore plus fluorite phases). For the RE_2MO_5 (M = Zr and Hf) stoichiometry, the structure is generally of defect fluorite type although short-range crystal structure modulations have been identified [8, 26, 27]. The rare earth stannates readily form pyrochlore for $RE_2Sn_2O_7$ stoichiometry [28] but have very limited solid solutions between the $RE_2Sn_2O_7$ and RE_2SnO_5 regions with only Yb_2SnO_5 having been identified as single phase [29].

Whilst there are a range of structure types available for the RE_2MO_5 system of compounds, the most promising from radiation response studies are those with cubic symmetry [9, 11, 15, 23, 24]. A general trend of improved radiation response, critical fluence of irradiating ions required for complete amorphisation, in those pyrochlores for which a transition to the fluorite structure is energetically favourable has been noted in several studies [2, 3, 15]. Ion irradiation studies on the $RE_2Ti_2O_7$ pyrochlore system (RE = Sm to Lu) have shown a general trend of improved radiation tolerance, greater critical fluence to facilitate a crystalline to amorphous transition, for those specimens with smaller radius lanthanides [30]. This improvement in radiation response has been associated with the ability to accommodate disorder, in this case mixing of cations across the available sites, along with anion disorder. This has been further investigated between $RE_2Ti_2O_7$ and RE_2TiO_5 stoichiometries with the RE_2TiO_5, a structure able to accommodate greater cation disorder, showing improved, increased critical fluence required for complete amorphisation, ion irradiation response [15]. In a separate ion irradiation, 2.2-GeV gold ions, in a study by Park et al. [31] on Nd_2TiO_5, Gd_2TiO_5, and Yb_2TiO_5 compounds, Yb_2TiO_5 was found to have the greatest tolerance, least susceptible to amorphisation of the compounds studied. Whilst not explicitly stated, the critical fluence for complete amorphisation, F_c, for the Yb_2TiO_5 compound appears to be 3×10^{13} ions/cm^2, extrapolated from the amorphous volume versus fluence plot. In a previous 2.2-GeV gold ion irradiation study on $Yb_2Ti_2O_7$, an F_c value of 1.5×10^{13} ions/cm^2, half of that found for the Yb_2TiO_5 compound, was determined [32]. For mixed cations such as the $RE_2M_2O_7$ systems, the compounds with cations of similar ionic radii tend to form more readily in the defect-fluorite structure rather than the pyrochlore. Those compounds that either have defect fluorite structure or can transition to the defect fluorite structure upon irradiation also tend to be the most irradiation tolerant [2]. The radiation tolerance is related, at the atomistic level, to the relatively low cation anti-site and anion Frenkel defect energies, and low-energy barriers to migration as determined via density functional theory and molecular dynamics simulations. This means that rare earth zirconates, stannates, and hafnates (cations with larger ionic radii than titanium) tend to maintain their crystalline structure when exposed to ion-irradiation with the exception of some larger lanthanides such as $La_2M_2O_7$ [33–36].

In our study, here we aim to create novel single-phase compounds of RE_2MO_5 or slightly off-stoichiometry $Yb_2Sn_{1+x}O_{5+2x}$. It was hoped that by fabricating these new compounds with their inherent vacancies and cation disorders, new materials with the desirable property of radiation tolerance will be discovered.

Methods

Fabrication

Bulk polycrystalline samples were synthesized via the conventional oxide route method. Stoichiometric quantities of the precursor oxides Yb_2O_3, Sm_2O_3, TiO_2, and SnO_2 (Sigma-Aldrich, 99.9% purity) were measured and mixed, with further milling and mixing with 12-mm yttria stabilised ZrO_2 balls carried out using cyclohexane as a dispersant. The

pellets were consolidated by 20-MPa uniaxial pressing followed by cold isostatic pressing at 250 MPa. Sintering was carried out at 1500 °C for 48 h using a heating and cooling rate of 5 °C/min.

Scanning electron microscopy

SEM specimens were prepared from sample fragments set in epoxy resin and surface polished (Struers Tegramin 25) using suspensions of sequentially smaller diamond grit down to a final polish of 0.5-micron grit. The specimens were then carbon coated. SEM imaging and microanalysis were carried out on a Zeiss Ultra Plus operated at 15 kV, with Oxford X-Max energy-dispersive x-ray (EDS) detector and Oxford Aztec EDS analysis software.

Transmission electron microscopy

TEM specimens were prepared by crushing grains via mortar and pestle into crystal fragments dispersed in ethanol. Suspensions of crystal fragments were transferred via pipette onto holey carbon film, supported on copper TEM grids. The crystal fragments were investigated in the TEM using a JEOL 2200FS operated at 200 kV. To confirm cation ratios and the homogeneous distribution of elements, the energy-dispersive x-ray spectroscopy (EDS), Oxford X-MAX detector, was used to collect spectra from at least 30 grains per sample. The EDS data was analysed via Oxford INCA software. This system was standardised using in-house single-phase ceramics via the Cliff-Lorimer k-factor method [37].

Laboratory x-ray diffraction (XRD)

Powdered samples, less than 10 microns, were analysed using powder XRD (PANalytical X'pert Pro diffractometer) with weighted Cu-Kα radiation (Kα1 = 1.54060 Å, Kα2 = 1.54443 Å, Kα1/Kα2 = 2). For the $Yb_2Sn_{1.125}O_{5.25}$ specimen, XRD data Rietveld analysis was carried out using the Rietica software [38].

Bulk sample ion-irradiation

Previous to ion irradiation, bulk specimens, 10 × 10 mm, were surface polished using various grades of diamond abrasive films, down to 0.5 micron for final polish. The specimens Yb_2TiO_5, Sm_2ZrO_5, and $Yb_2Sn_{1.25}O_{5.5}$ were irradiated using the ANTARES TANDEM accelerator, ANSTO [39]. Each specimen received four different fluences: 1×10^{14}, 2×10^{14}, 5×10^{14}, and 7.5×10^{14} Au^+ at 15-MeV ions/cm^2.

Grazing incidence x-ray diffraction (GIXRD)

The ion-irradiation response of the tested ceramics was investigated via GIXRD. The x-ray diffraction was carried out on a Bruker D8 Advance diffractometer using a weighted Cu-Kα source. The x-ray angle of incidence was set at two different angles 3 and 5° with data collected between 10 and 90° 2-theta.

Damage simulation (stopping range of ions in solids, SRIM)

To model the ion irradiation damage depth profiles, the software SRIM was employed [40]. The set parameters included setting all displacement energies to 50 eV [41], lattice binding energies to 0 eV [42], and sample densities were set either according to previously published crystal structure data [8, 43] or based on the refined structure from this study. The SRIM simulations were calculated in the "ion distribution and quick calculation of damage" mode.

Results and discussion

The RE_2MO_5 compound series

Attempts were made to fabricate single-phase bulk ceramics with RE_2MO_5 stoichiometry. The complete reactions of precursors and subsequent formation of single-phase material with Yb_2TiO_5 stoichiometry were achieved (Fig. 1a). For the samarium zirconate, there were regions of minor deviation in elemental distribution from the target Sm_2ZrO_5 matrix composition (Fig. 1b). Based on visual analysis of SEM AsB imaging, the secondary phase constituted less than 10% by volume of the overall structure and had, based on EDS analysis, less than 10% atomic variation in zirconium (greater concentration when compared with the matrix). This result may be either indicative of incomplete precursor reaction or the formation of a more stable compound with stoichiometry between Sm_2ZrO_5 and $Sm_2Zr_2O_7$. Previous studies have shown that greater sintering temperatures, sometimes 1800 °C or above, may be required to achieve adequate reaction between RE_2O_3 and ZrO_2 precursors [44]. In a previous study by the authors, complete reaction of the precursors was achieved at a relatively lower sinter, 1400 °C, by using a wet-chemistry approach that allowed mixing of the precursors at the molecular level [8]. In our fabrication approach for this current study, we have used the conventional mixing of oxide precursors approach for ease of preparation.

Whilst there are numerous publications on $RE_2Sn_2O_7$ pyrochlores, there are only very limited studies on RE_2SnO_5. In a previous study by the authors, various combinations of RE_2SnO_5 were attempted and found to

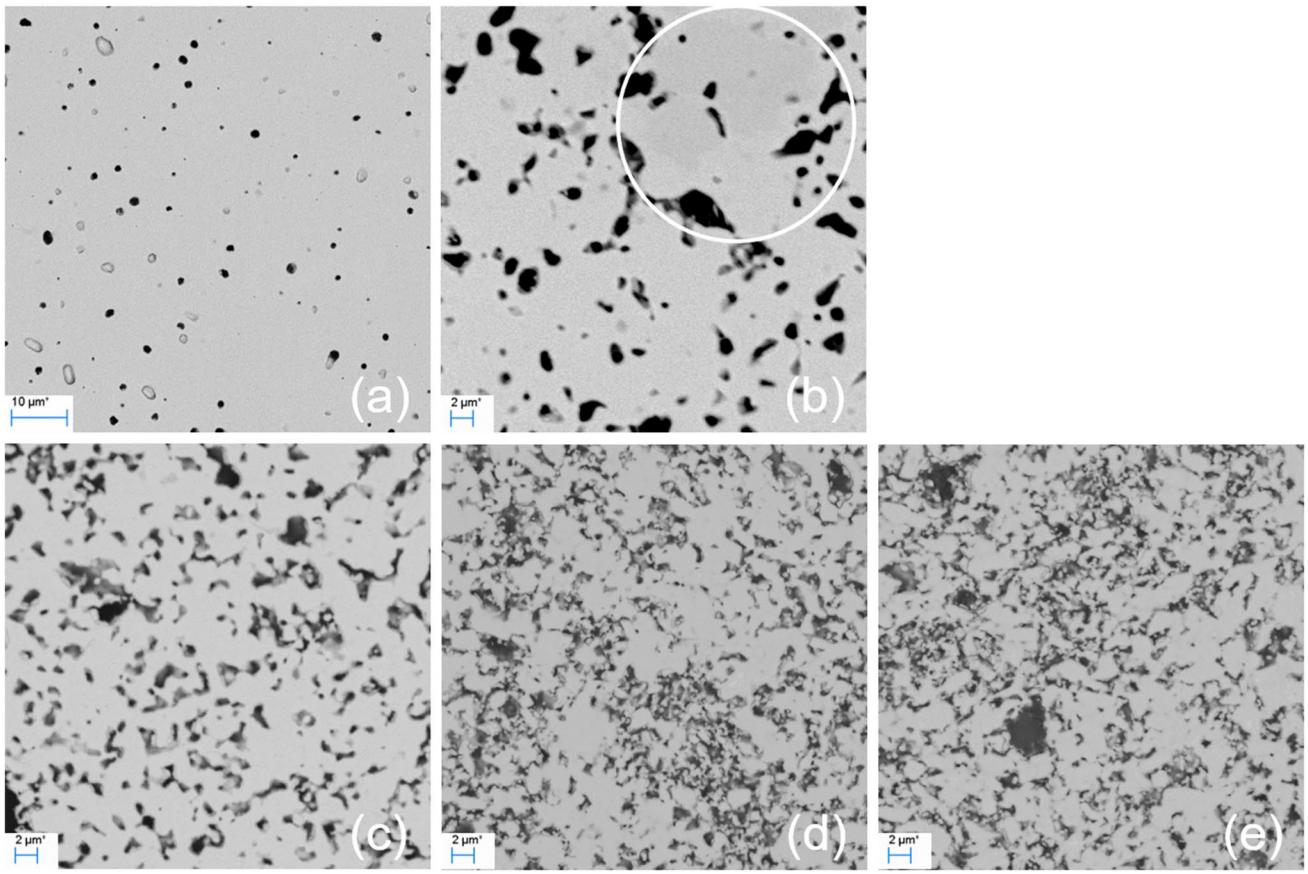

Fig. 1 SEM annular selective backscattered (AsB) images showing homogeneity of elemental distribution (variation in contrast indicates uneven elemental distribution) for each of the ceramics studied; **a** Yb_2TiO_5, **b** Sm_2ZrO_5 with circle highlighting area with minor contrast variation, **c** $Yb_2Sn_{1.125}O_{5.25}$, **d** $Yb_2Sn_{1.25}O_{5.5}$, and **e** $Yb_2Sn_{1.375}O_{5.75}$. Dark regions are pores. Image (**a**) is of lower magnification (note 10-micron scale bar) relative to other images (2-micron scale bar)

generally form multiple stoichiometry phased materials [29]. Whilst a single-phase Yb_2SnO_5 was not realised, the relatively small volume of precursor found as a secondary phase prompted attempts at fabricating single-phase materials with slightly greater tin content. Successful fabrication of single-phase materials with stoichiometry $Yb_2Sn_{1.125}O_{5.25}$, $Yb_2Sn_{1.25}O_{5.5}$, and $Yb_2Sn_{1.375}O_{5.75}$ (Fig. 1c, d, and e) has been achieved. The stannates fabricated here have a relatively porous structure, like the Sm_2ZrO_5, whilst the Yb_2TiO_5 has formed with minimal porosity (Fig. 1). This may be related to the highly refractory nature of the SnO_2 and ZrO_2 precursors when compared with TiO_2. Due to the porous nature of the stannate and zirconate samples, elemental analysis via the TEM EDS method was utilised. The determined stoichiometries, with errors based on two standard deviations, shown in brackets, were as follows; $Yb_{2.00(0.03)}Ti_{1.01(0.03)}O_{5.01(0.01)}$, $Sm_{2.00(0.06)}Zr_{1.16(0.07)}O_{5.32(0.01)}$, $Yb_{2.00(0.10)}Sn_{1.12(0.07)}O_{5.24(0.01)}$, $Yb_{2.00(0.26)}Sn_{1.32(0.19)}O_{5.63(0.02)}$, and $Yb_{2.00(0.28)}Sn_{1.56(0.20)}O_{6.11(0.02)}$. The average measured cation ratios for all compounds were found to be close to the nominal stoichiometries, within statistical error. However, there may be some variation in elemental distribution, as indicated by the distribution of measured values, for the $Yb_2Sn_{1.25}O_{5.5}$ and $Yb_2Sn_{1.375}O_{5.75}$ samples.

As there is limited information on structures with the RE_2SnO_5 stoichiometry, we sought to refine, via the Rietveld method [38], the XRD data for the stannate series; $Yb_2Sn_{1.125}O_{5.25}$, $Yb_2Sn_{1.25}O_{5.5}$, and $Yb_2Sn_{1.375}O_{5.75}$. The refinement of XRD data for the $Yb_2Sn_{1.125}O_{5.25}$ specimen (Fig. 2, Table 1) showed a cell parameter $a = 5.17233$ (1) for the symmetry group *Fm*-3 *m*. The cell parameter is slightly greater than the similarly structured Yb_2TiO_5, previously published, $a = 5.09418$ (9) [43], but significantly less than that previously determined for Sm_2ZrO_5, $a = 5.35795$ (1) [8]. These variations in cell parameters may be explained using differences in cation ionic radii based on those values proposed by Shannon [45]. For Sn^{4+} (VIII) $R_I = 0.81$ whilst Ti^{4+} (VIII) $R_I = 0.74$, and this would allow the Yb_2TiO_5 fluorite-structured matrix to occupy a smaller volume when compared with $Yb_2Sn_{1.125}O_{5.25}$. For the samarium zirconate

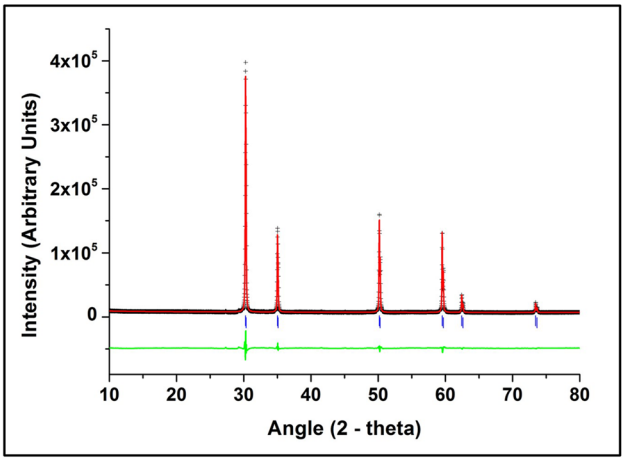

Fig. 2 XRD pattern for the $Yb_2Sn_{1.125}O_{5.25}$ sample. The collected data points are displayed as black crosses, whilst the calculated (Rietveld refinement) values are overlaid as the red trace. The difference in value between the data and refinement (residual) is shown as the green trace below the data and calculated fit. The positions of reflections are marked by blue markers below the plot

Table 1 The Rietveld refinement of powder XRD data, calculated values for $Yb_2Sn_{1.125}O_{5.25}$. The refinement was based on *Fm*-3 *m* symmetry with cell parameter $a = 5.17233$ (1), and statistics of fit Rp = 3.07%, Rwp = 4.09%, and $X^2 = 16.5$

Element	x	y	z	Uiso*100	Occupancy
Yb^{3+}	0	0	0	1.81 (2)	64
Sn^{4+}	0	0	0	1.81 (2)	36
O^{2-}	0.25	0.25	0.25	6.3 (1)	84

compound, both Sm^{3+} (VIII) $R_I = 1.079$ is greater than Yb^{3+} (VIII) $R_I = 0.985$, and Zr^{4+} (VIII) $R_I = 0.84$ is greater in size than both Sn and Ti.

Finding a bulk material, rare earth stannate with fluorite-type structure is unique. In a previous study, using ^{119}Sn MAS NMR, looking at the local crystal structure for $Y_2Ti_{2-x}Sn_xO_7$ pyrochlores, it was found that Sn always resided on the pyrochlore B-site [46]. The significance of this result is that tin, having a relatively large ionic radius close to the rare earths, may be expected to result in a range of fluorite/pyrochlore structures, and up to the time of this study, this has not been found. Zirconium has been noticed to substitute onto the A site in the $RE_2M_2O_7$ form for smaller cationic radii ratios such as yttrium whilst tin maintains its' B-site position [47].

Attempts were made to also refine the XRD data for the two remaining stannate samples for this study. However, it was noted that extra peaks were present (Fig. 3) for the $Yb_2Sn_{1.25}O_{5.5}$ and $Yb_2Sn_{1.375}O_{5.75}$ samples. Whilst SEM analysis (Fig. 1) and TEM EDS analysis indicated that these compositions were of a single stoichiometry, homogeneous distribution of the elements, the splitting of the reflection peaks for the $Yb_2Sn_{1.25}O_{5.5}$ and $Yb_2Sn_{1.375}O_{5.75}$ samples (Fig. 3) indicates a 2 phase (structure). The crystal structures for these two compounds could be refined approximately, based on the *Fm*-3 *m* symmetry, although they require a two-phase refinement for proper fitting. It is for this reason refinements based on the LeBail method [48] were used for the $Yb_2Sn_{1.25}O_{5.5}$ and $Yb_2Sn_{1.375}O_{5.75}$ stoichiometries.

Fluorite-modulated structure

Whilst the x-ray diffraction results (Fig. 3) show the long-range structure, within the coherence length of x-rays, can be defined using fluorite *Fm*-3 *m* symmetry, previous studies on RE_2ZrO_5 [8, 26, 27] and RE_2TiO_5 [15, 25, 43] have shown complex structural modulations exist, detected via electron diffraction. In Fig. 4, we show a series of selected area electron diffraction patterns from the compounds Sm_2ZrO_5, $Yb_2Sn_{1.125}O_{5.25}$, and Yb_2TiO_5 together with two simulated diffraction patterns for reference, all shown down zone axis [1 1 0]. The simulated reference patterns are shown in Fig. 4a and b and show the lattice points and indices for pyrochlore and defect fluorite, respectively. The observed [1 1 0] zone axis electron diffraction patterns for Sm_2ZrO_5, $Yb_2Sn_{1.125}O_{5.25}$ and Yb_2TiO_5 are shown in Fig. 4c, d, and e, respectively. By reference to the pyrochlore pattern in Fig. 4a, we see that all three of the observed patterns exhibit strong scattering for the conditions $h = 2n$, $k = 2n$, and $l = 2n$ (all even). The observed patterns for all three samples also show diffuse scattering on (or near) pyrochlore lattice points with *h*, *k*, and *l* all odd. For Sm_2ZrO_5, the scattering appears as small, round, diffuse spots lying directly on the odd (pyrochlore) lattice points. In comparison, $Yb_2Sn_{1.125}O_{5.25}$ shows pairs of small diffuse spots lying on either side of the odd-numbered lattice points, denoted as $G_F \pm ½(111)$*. This scattering is typical of the pyrochlore to defect fluorite transformation observed in other compositions [27, 47, 49]. In the case of Yb_2TiO_5, we find diffuse scattering in the form of small rectangular blocks that are elongated in the < 111 > directions. This scattering is atypical of the "227"-type pyrochlore to defect fluorite transformation and probably relates to the different stoichiometry of this "215"-type compound.

The collection of bright-field high-resolution images (HREM) via TEM (Fig. 5) for the Sm_2ZrO_5 compound highlights the presence of nano-domains. The HREM has been converted to a fast Fourier Transform (FFT) (Fig. 5b), highlighting the symmetry within Fig. 5a. This symmetry matches the reflection positions found within the electron diffraction pattern when viewed down zone axis [1 1 0] (Fig. 4a and c) for pyrochlore *Fd*-3 *m* symmetry. It should be noted that whilst the FFT symmetry matches that of pyrochlore-type structure, the modulations

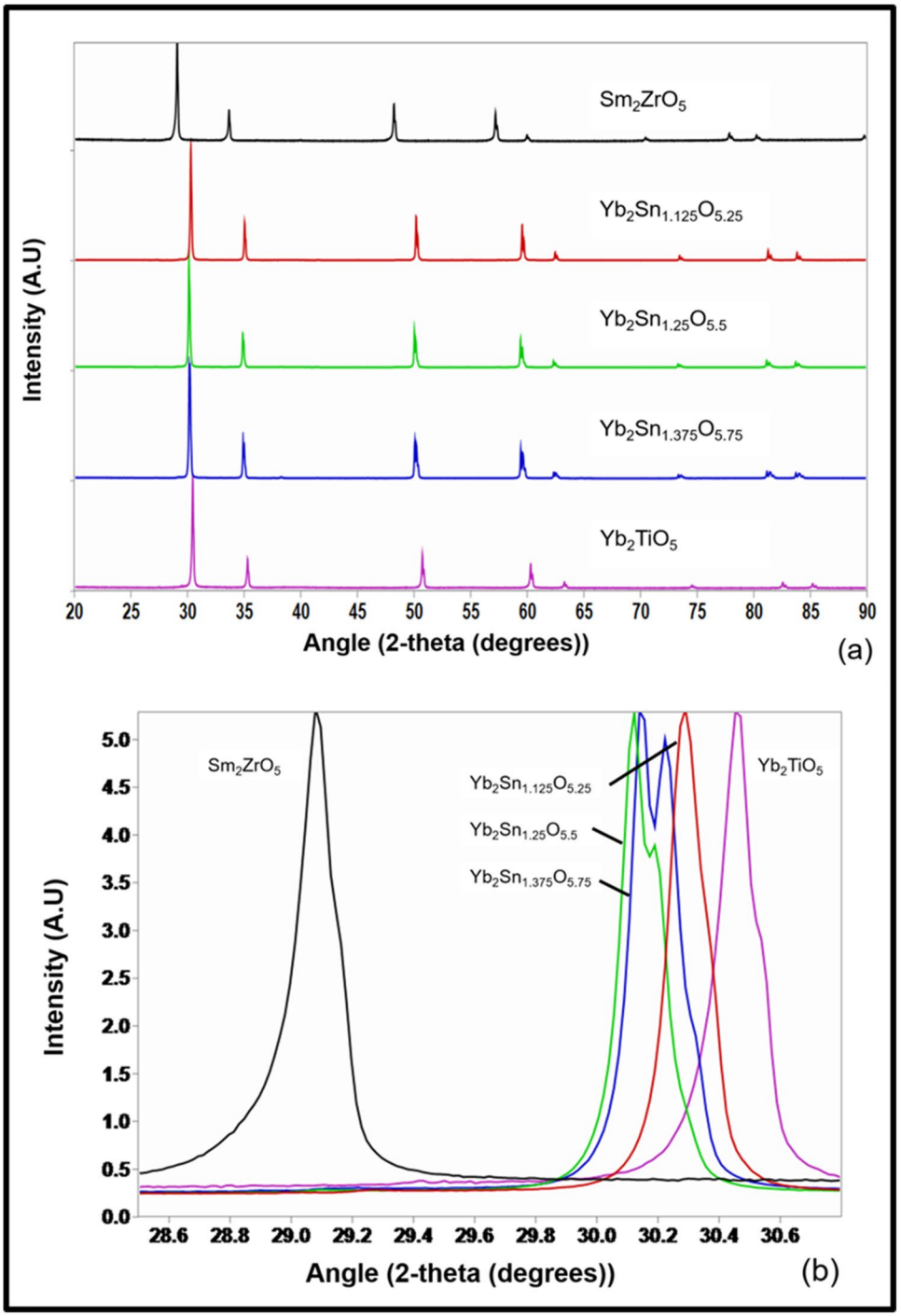

Fig. 3 XRD patterns for the five ceramics of interest; Sm_2ZrO_5, Yb_2TiO_5, $Yb_2Sn_{1.125}O_{5.25}$, $Yb_2Sn_{1.25}O_{5.5}$, and $Yb_2Sn_{1.375}O_{5.75}$, with patterns normalised and offset in (**a**) for comparison. All diffraction patterns have reflections matching *Fm*-3 *m* symmetry. **b** shows the (1 1 1) *Fm*-3 *m* reflection for each ceramic specimen

detected in the electron diffraction of Fig. 4c are not evident in the FFT. The detection of (1 1 1) reflections related to pyrochlore-type structure for the Sm_2ZrO_5 compound, as found in Fig. 4c and 5b, was previously not detected in the XRD data (Fig. 3). This is likely due to the coherence length of electron diffraction being smaller than that for x-ray diffraction. Masking all points except those related to the (1 1 1) pyrochlore reflection in Fig. 5b and then inverting the FFT, nano-domains of 2- to 5-nm diameter can clearly be seen in Fig. 5d. In a previous study, it has been shown that for the Yb_2TiO_5 compound, altering the sintering conditions to encourage the nano-domains of pyrochlore-type structure to grow a critical domain size can be reached above which pyrochlore related reflections can be detected within XRD patterns [24].

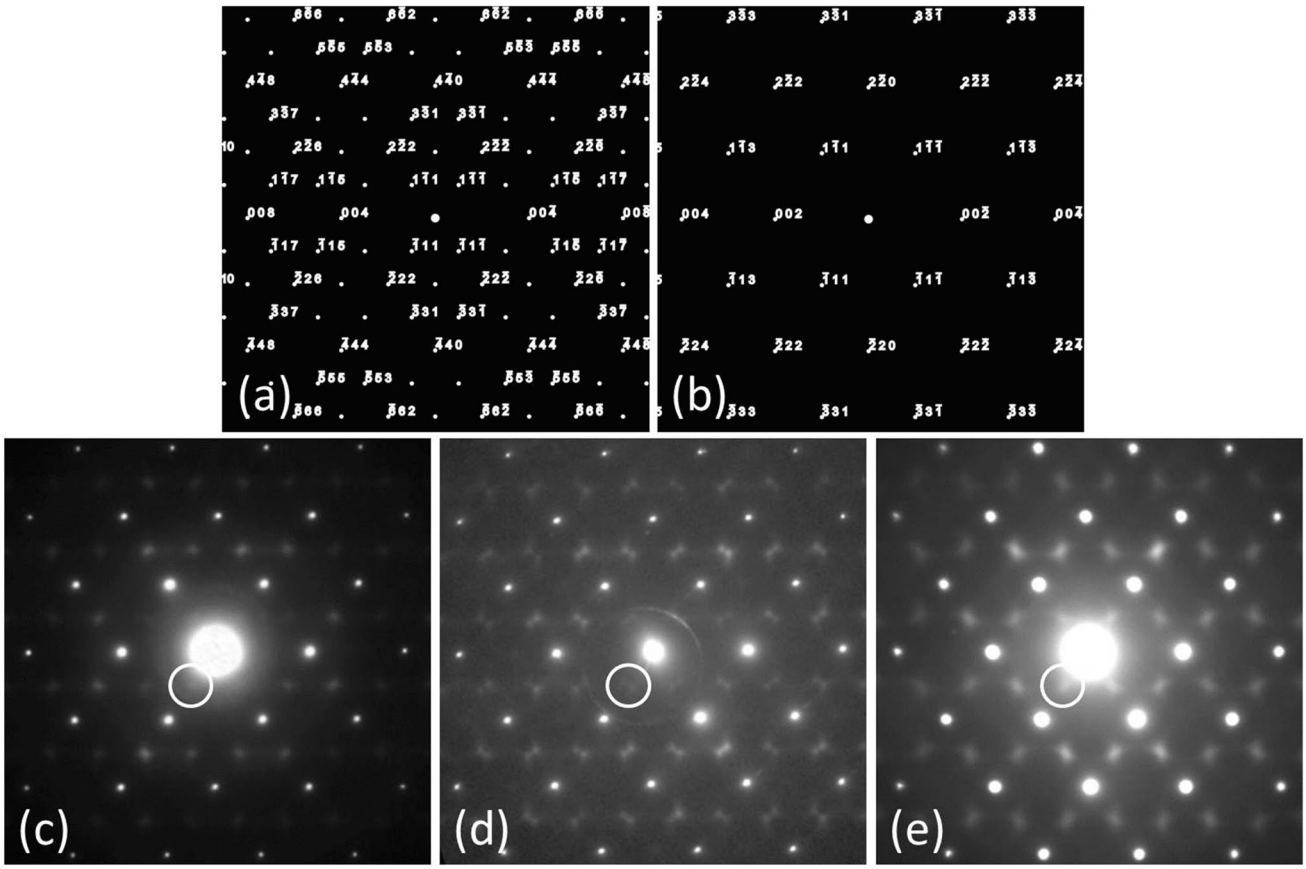

Fig. 4 Series of selected area electron diffraction patterns from three cubic compounds (Sm_2ZrO_5, $Yb_2Sn_{1.125}O_{5.25}$, and Yb_2TiO_5) fabricated for this study. The two simulated diffraction patterns, shown down zone axis [1 1 0], **a** and **b** are from pyrochlore and fluorite structures, respectively. Selected area electron diffraction patterns, also shown down zone axis [1 1 0], **c**, **d**, and **e** are from Sm_2ZrO_5, $Yb_2Sn_{1.125}O_{5.25}$, and Yb_2TiO_5, respectively. The diffuse scattering from the (1 1 1) equivalent pyrochlore plane is highlighted via a circle in each of the collected SADPs

Ion-irradiation tolerance

The complete Rietveld refinement of XRD data for all ytterbium stannate compounds in our study was not carried out to completion due to the 2-phase (crystal structure variation) nature of the $Yb_2Sn_{1.25}O_{5.5}$ and $Yb_2Sn_{1.375}O_{5.75}$ compounds (Fig. 3). However, for x-ray penetration depth and ion irradiation damage depth profile calculations, an estimate of the $Yb_2Sn_{1.25}O_{5.5}$ structure was required. The calculated, Le Bail method [48], cell parameter for $Yb_2Sn_{1.25}O_{5.5}$ was $a = 5.17498$ (8) Å and this gave a theoretical density of 8.71 g/cm^3 (Table 2). The calculated, Le Bail method, cell parameter for $Yb_2Sn_{1.375}O_{5.75}$ was $a = 5.1516$ (1) Å.

The greater density of the $Yb_2Sn_{1.25}O_{5.5}$ sample leads to greater x-ray attenuation relative to the Yb_2TiO_5 sample. However, the presence of samarium, and its mass attenuation co-efficient, for the Sm_2ZrO_5 compound leads to a significant decrease in x-ray penetration relative to the other compounds studied (Table 2). Bulk irradiated specimens were analysed using grazing incidence x-ray diffraction (GIXRD) with the incidence angle set at 3 and 5°. The x-ray penetration depths were calculated using the software Panalytical HighScore [50] (Fig. 6)

The use of two different incident angles for the x-rays has allowed different depths below the irradiated surface to be sampled from (Table 2). For the 15-MeV gold ion irradiation of bulk Yb_2TiO_5, there appears to be nearly complete amorphisation at the maximum fluence of 7.5×10^{14} ions/cm^2 (Fig. 7a) from the surface to 1.217 micron depth (Table 2). When the x-ray incident angle was increased to 5° (Fig. 7b), x-ray penetration depth to 2.028 micron (Table 2), some reflections from the crystalline phase are still apparent up to the maximum fluence used. For this higher x-ray incidence angle, the x-rays are sampling beyond the depth of calculated peak ion-irradiation damage, 1.71 micron (Table 2). Whilst the calculated peak damage depth is at a maximum level of damage, displaced lattice atoms, at 1.71 micron there is still a relatively large number of displaced lattice atoms up to and just beyond a depth of 2.028 micron (Fig. 6). There are two main possible explanations for crystalline material being

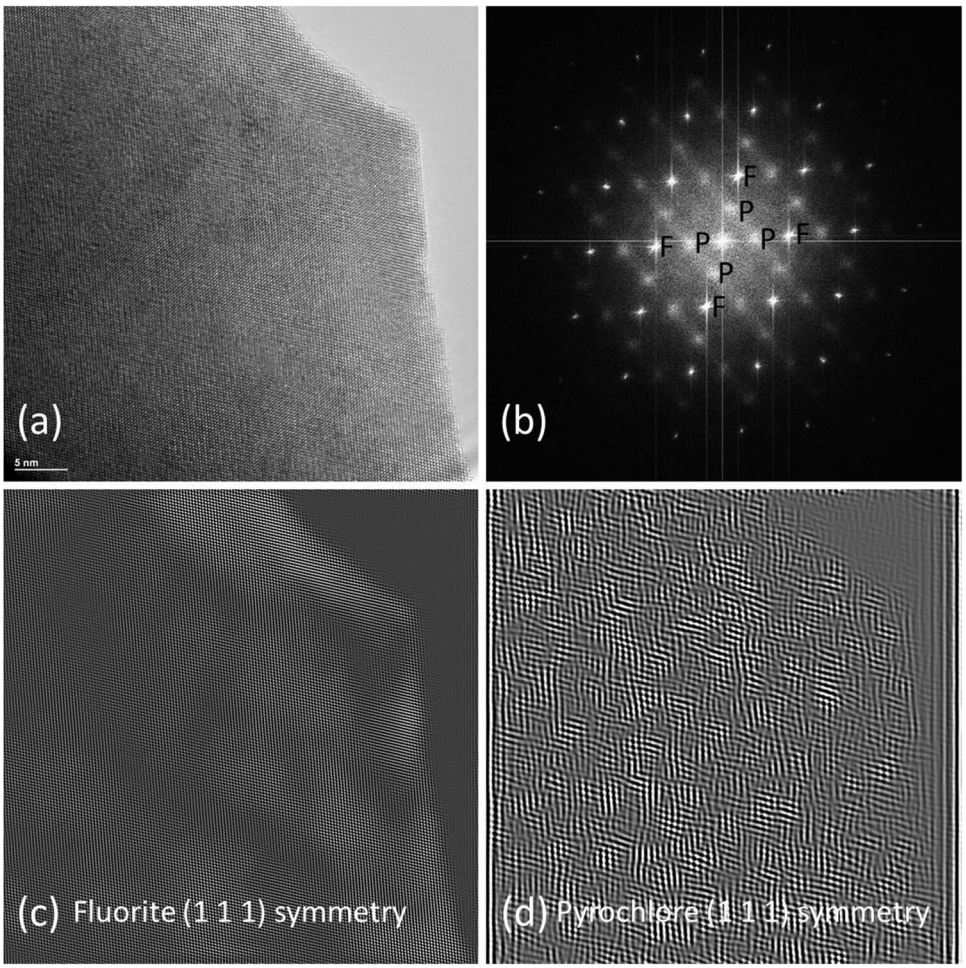

Fig. 5 The high-resolution bright field image of Sm_2ZrO_5 orientated down zone axis [1 1 0] to highlight lattice contrast is shown in (**a**) with a fast Fourier transform (FFT) of this shown in (**b**). The FFT in (**b**) has the symmetry equivalent to (1 1 1) pyrochlore planes marked with "P" (to the right of each) and symmetry equivalent to (1 1 1) fluorite marked with "F". Inverse FFT images were created by masking everything in the FFT except the symmetry relevant to either the (1 1 1) fluorite (**c**) or (1 1 1) pyrochlore (**d**) and then inverting the FFT. The 5-nm scale bar in (**a**) can be used as a guide for the inverted FFT images in (**c** and **d**)

Table 2 The calculated x-ray (copper k-alpha) penetration depths [50], ion irradiation–induced damage depth profile [40], and density based on determined crystal structure refinements

Compound	X-ray penetration depth—microns (3 deg. incidence)	X-ray penetration depth—microns (5 deg. incidence)	Peak damage depth (microns)	Density (g/cm^3)
Yb_2TiO_5	1.217	2.028	1.71	7.67
$Yb_2Sn_{1.25}O_{5.5}$	0.893	1.487	1.56	8.71
Sm_2ZrO_5	0.539	0.897	1.95	6.77

detected, even up to maximum fluence, via GIXRD of 5°; x-ray penetration depths and damage depth calculations are both based on simple simulations so are only estimations, and bulk specimens may behave differently between their surface and internal properties. The ion-irradiation behaviour of thin crystals and bulk specimens has been shown to have similar trends but different values due to differences in the surface to volume ratios [23].

Whilst the maximum fluence of 15-MeV gold ions, 7.5×10^{14} ions/cm^2, was sufficient to render a certain volume of the Yb_2TiO_5 amorphous, there appears to be little damage to either of the Sm_2ZrO_5 or $Yb_2Sn_{1.25}O_{5.5}$ specimens tested (Figs. 8 and 9). In fact, there was no measurable shift in peak positions with increasing fluence for the Sm_2ZrO_5 sample (Fig. 8). In a previous transmission electron microscopy in situ ion irradiation study by the authors on several RE_2ZrO_5 compounds, the crystal structures were generally unchanged between pre- and post-irradiation [8].

There was some shifting of reflection peak positions with fluence for the $Yb_2Sn_{1.25}O_{5.5}$ specimen (Fig. 9) to lower angle indicating a volume increase with exposure to ion irradiation. There was no indication of any ion irradiation–induced crystal structure change even up to maximum fluence.

The ion irradiation response for the $RE_2Sn_2O_7$ system studied via in situ (TEM) irradiation by Lian et al. [51]

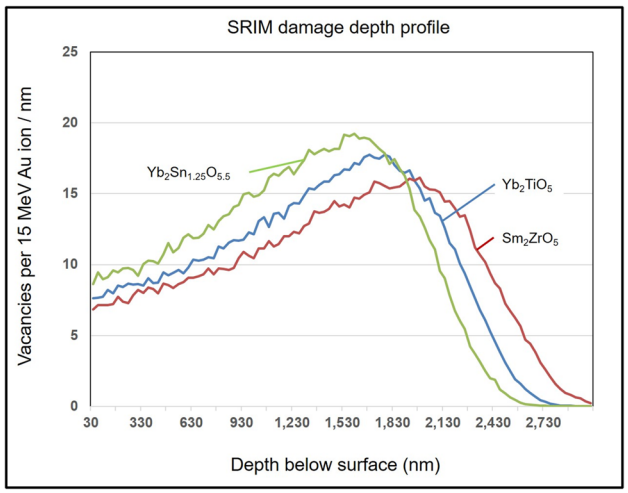

Fig. 6 The calculated, from SRIM simulation, damage depth profiles for the three irradiated, 15 MeV Au^{+} ions, specimens in this study

showed an improvement in radiation response with decreasing rare earth size with $Er_2Sn_2O_7$ maintaining crystallinity regardless of 1-MeV Kr fluence even when held at 25 K. Whilst the entire series of $RE_2Sn_2O_7$ compounds have been identified as pyrochlores with *Fd*-3 *m* symmetry [28], it may be possible for those stannate compounds with smaller sized rare earths to undergo an irradiation-induced transition from pyrochlore to fluorite-type structure [52]. The ability of zirconate pyrochlores to undergo a transition from pyrochlore to fluorite has previously been highlighted as a source of improved radiation tolerance [53]. For the $Yb_2Sn_{1.25}O_{5.5}$ compound studied here, the fact that the long-range structure has been identified as fluorite-type may be a contributing factor to its ability to maintain crystallinity during exposure to high energy 15 MeV, heavy ions, Au + (Fig. 9).

Stannates, when compared with titanates and zirconates, possess a less ionic metal–oxygen bond in accordance with the lesser electronegativity difference between the metal and oxygen ions. This strengthens the attraction between tin cations and oxygen anions, creating a more covalent-type bond, something that has been supposed to be detrimental to maintenance of crystal structure with exposure to irradiation [54]. Sn–O bonding and the electrical potential wells resulting forms an impediment to the ion movement required for recrystallization [55]. Contrary to these previous studies, the increased covalency found in Sn–O bonding does not appear to play the dominant role in determining the resistance to amorphisation found in our $Yb_2Sn_{1.25}O_{5.5}$ sample. Previous experimental and simulation [2, 51]-based studies have shown cation ionic radii (r_{RE}/r_M) of similar sizes tend to be less susceptible to amorphisation when compared with greater cation size mismatches. Also, by altering the local Sn–O co-ordination number from 6 (octahedron) to 8 (distorted cube) through the transition from pyrochlore to fluorite-type structure, as has been achieved for the $Yb_2Sn_{1.25}O_{5.5}$ sample studied here, there will be a resulting change to the bonding, possibly making it less directional and so less covalent in nature.

Titanate pyrochlores, $RE_2Ti_2O_7$, have been shown to be susceptible to ion irradiation–induced amorphisation [56, 57]. A general trend of improved radiation response, higher critical fluence required for amorphisation, was observed for rare earths of smaller ionic size with ytterbium and lutetium titanates showing the greatest radiation tolerance [30]. A further improvement in radiation

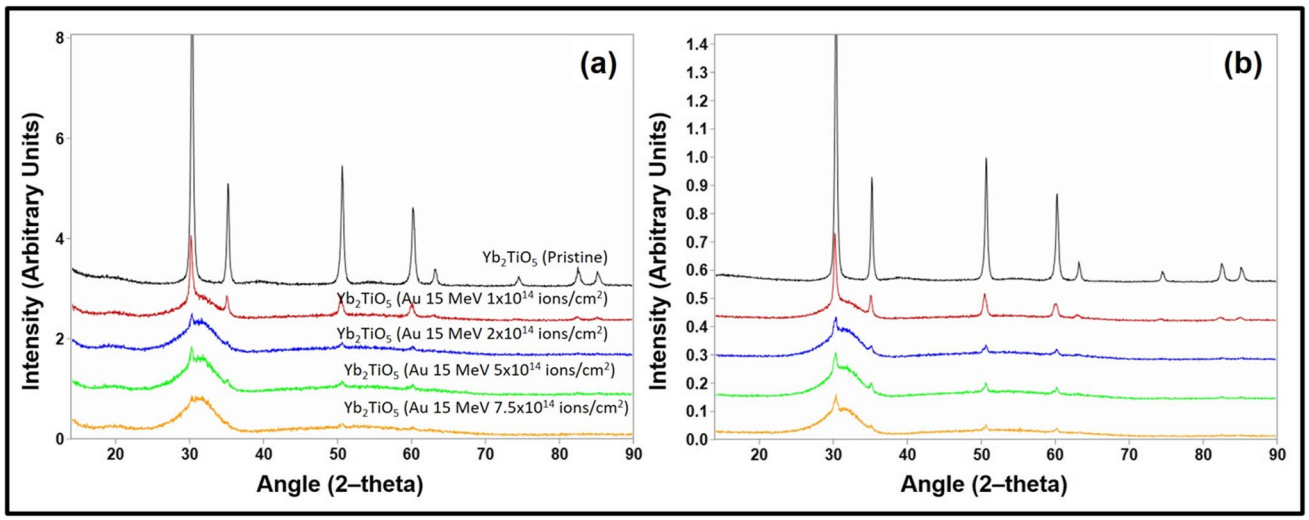

Fig. 7 GIXRD patterns for bulk irradiated, 15-MeV Au ions, Yb_2TiO_5 specimen. The diffraction patterns have been offset from each other for clarity with the pattern taken for the pristine, unirradiated specimen shown at top and patterns from sequentially greater fluences (1, 2, 5, and 7.5×10^{14} ions / cm^2) shown below. Patterns in (**a**) were taken using 3 degrees angle of incidence, (**b**) 5 degrees

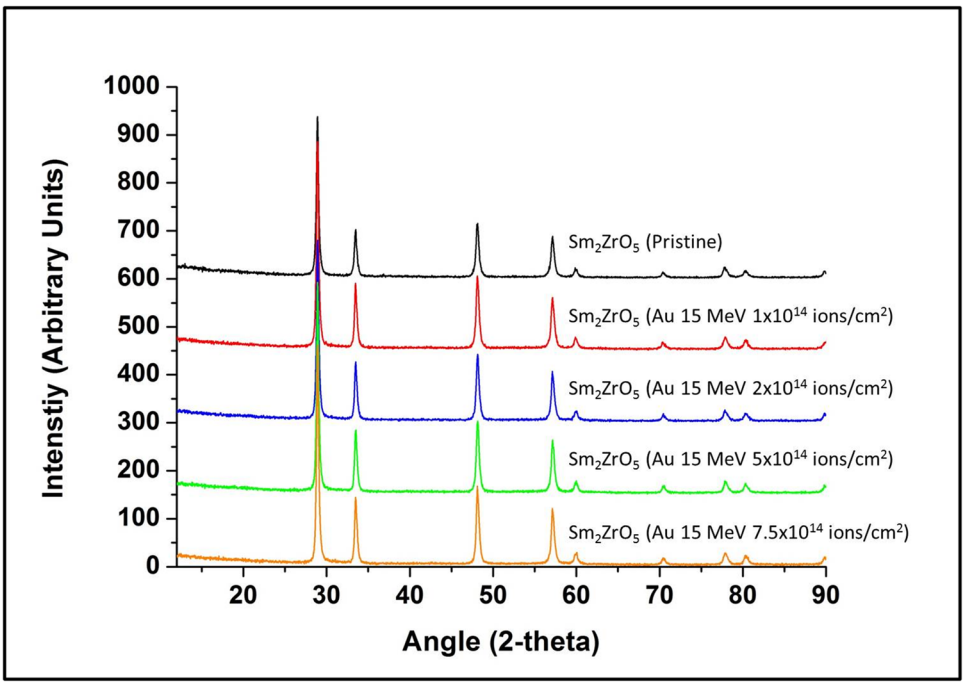

Fig. 8 GIXRD, 5 degrees angle of incidence, patterns for bulk irradiated, 15-MeV Au ions, Sm_2ZrO_5 specimen. The diffraction patterns have been offset from each other for clarity with the pattern taken for the pristine, unirradiated specimen shown at top and patterns from sequentially greater fluences (1, 2, 5, and 7.5×10^{14} ions / cm^2) shown below

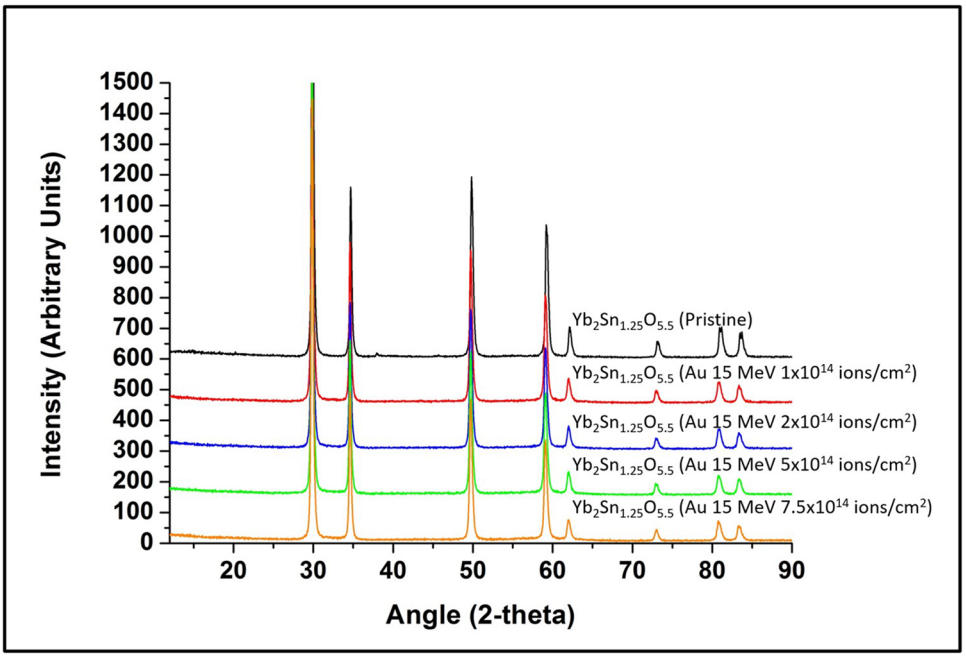

Fig. 9 GIXRD, 5 degree angle of incidence, patterns for bulk irradiated, 15 MeV Au ions, $Yb_2Sn_{1.25}O_{5.5}$ specimen. The diffraction patterns have been offset from each other for clarity with the pattern taken for the pristine, unirradiated specimen shown at top and patterns from sequentially greater fluences (1, 2, 5, and 7.5×10^{14} ions / cm^2) shown below

tolerance was discovered when moving from $RE_2Ti_2O_7$ to RE_2TiO_5 stoichiometry [15]. Based on these previous ion irradiation studies, it seemed reasonable to predict that the $Yb_2Sn_{1.25}O_{5.5}$ and Sm_2ZrO_5 compounds should maintain crystallinity when exposed to 15-MeV gold ions and this is what has been found (Figs. 8 and 9), whilst the more radiation damage susceptible Yb_2TiO_5 compound is seen to undergo a crystalline to amorphous transition with increasing fluence (Fig. 7a).

Based on the GIXRD, 3 degrees angle of incidence, (Fig. 7a) where complete amorphisation is achieved at the maximum fluence of 7.5×10^{14} Au ions/cm^2, and the calculated damage depth profile (Fig. 6), the approximate critical fluence for amorphisation for the Yb_2TiO_5 compound is 0.71 displacements per atom (dpa). The actual critical fluence, F_c, may be lower than this as the diffraction data comes from the surface to approximately 1.2-micron depth when using the 3 degrees angle of incidence. However, this

dpa value matches well with that determined in a previous bulk irradiation study where the Yb_2TiO_5 compound was irradiated with 1-MeV Se ions where the F_c was determined to be 0.79 dpa [23]. The F_c value in our study does differ from that found using the in situ approach, 1-MeV Kr ions, of 0.55 dpa in the previous study [23]. However, variation in the determined critical fluence when comparing results from in situ (thin crystal fragments) and ex situ bulk irradiations may be due to epitaxial re-crystallisation found for bulk specimens, especially when irradiation occurs close to the critical temperature [23].

Conclusion

Novel, new compounds $Yb_2Sn_{1.125}O_{5.25}$, $Yb_2Sn_{1.25}O_{5.5}$, and $Yb_2Sn_{1.375}O_{5.75}$ have been fabricated as well as Sm_2ZrO_5 and Yb_2TiO_5. These compounds add to the family of defect fluorite–type structured materials with the general stoichiometry of RE_2MO_5. Whilst the average, long-range structure may be defined as fluorite with *Fm*-3 *m* symmetry, TEM analysis shows a much more complex, modulated crystal structure for all compounds studied here. These modulations may be described via the pyrochlore structure; however, diffraction patterns show incommensurate modulations from the ideal pyrochlore-type structure. As with previous related ion irradiation studies, the defect fluorite–structured materials tend to show resistance to amorphisation when exposed to ion irradiation making them ideal candidates for nuclear fuel cycle–related applications.

Acknowledgements The authors wish to thank Tim Palmer, NMDC, metallography, ANSTO, for his SEM specimen preparation.

Declarations

Competing interests The authors declare no competing interests.

References

1. Uberuaga, B.P., et al.: Opposite correlations between cation disordering and amorphization resistance in spinels versus pyrochlores. Nat. Commun. **6**(1), 8750 (2015)
2. Lumpkin, G.R., et al.: Nature of the chemical bond and prediction of radiation tolerance in pyrochlore and defect fluorite compounds. J. Solid State Chem. **180**(4), 1512–1518 (2007)
3. Sickafus, K.E., et al.: Radiation-induced amorphization resistance and radiation tolerance in structurally related oxides. Nat. Mater. **6**(3), 217–223 (2007)
4. Van Dijk, M., K. De Vries, A.J.S.S.I: Burggraaf, Oxygen ion and mixed conductivity in compounds with the fluorite and pyrochlore structure. **9**: 913–919 (1983)
5. Lian, J., et al: Nanoscale manipulation of pyrochlore: new nanocomposite ionic conductors. **87**(14), 145901 (2001)
6. Subramanian, M., G. Aravamudan, G.S.J.P.i.S.S.C. Rao: Oxide pyrochlores—a review. **15**(2), 55–143 (1983)
7. Andrievskaya, E.: Phase equilibria in the refractory oxide systems of zirconia, hafnia and yttria with rare-earth oxides. J. Eur. Ceram. Soc. **28**(12), 2363–2388 (2008)
8. Aughterson, R. D., G.R.L., Zhang, Z., Avdeev, M., Kong, L: Crystal chemistry and ion-irradiation resistance of Ln2ZrO5 compounds with Ln = Sm, Eu, Gd and Tb. Manuscript submitted for publication (2021)
9. Risovany, V., Varlashova, E., Suslov, D.: Dysprosium titanate as an absorber material for control rods. J. Nucl. Mater. **281**(1), 84–89 (2000)
10. Aughterson, R.D., N.J. Zaluzec, G.R. Lumpkin, Synthesis and ion-irradiation tolerance of the Dy2TiO5 polymorphs. Acta Materialia, **204**, 116518 (2021)
11. Aughterson, R.D., et al.: The influence of crystal structure on ion-irradiation tolerance in the Sm(x)Yb(2–x)TiO5 series. J. Nucl. Mater. **471**, 17–24 (2016)
12. Aughterson, R.D., et al.: Ion-irradiation resistance of the orthorhombic Ln2TiO5 (Ln = La, Pr, Nd, Sm, Eu, Gd, Tb and Dy) series. J. Nucl. Mat **467**(2), 683–691 (2015)
13. Zhang, J., et al.: Ion-irradiation-induced structural transitions in orthorhombic Ln2TiO5. Acta Mater. **61**(11), 4191–4199 (2013)
14. Tracy, C.L., Liang, M., Zhang, J., Zhang, F., Wang, Z., Ewing, R.C.: Structural response of A2TiO5 (A=La, Nd, Sm, Gd) to swift heavy ion irradiation. Acta Mater. **60**(11), 4477–4486 (2012)
15. Whittle, K.R., et al.: Ion irradiation of novel yttrium/ytterbium-based pyrochlores: The effect of disorder. Acta Mater. **59**(20), 7530–7537 (2011)
16. Whittle, K.R., et al.: Ion-beam irradiation of lanthanum compounds in the systems La2O3–Al2O3 and La2O3–TiO2. J. Solid State Chem. **183**(10), 2416–2420 (2010)
17. Pramudita, J.C., et al: Using in situ synchrotron x-ray diffraction to study lithium-and sodium-ion batteries: a case study with an unconventional battery electrode (Gd_2TiO_5). J. Mat. Res, 1–9 (2014)
18. Pan, T.M., Lin, C.W.: High-kappa Dy2TiO5 Electrolyte-Insulator-Semiconductor Urea Biosensors. J. Electrochem. Soc. **158**(4), J100–J105 (2011)
19. Kao, C.H., Chen, H.A., Lin, S.P.: The comparison of the high-k Sm2O3 and Sm2TiO5 dielectrics deposited on the polycrystalline silicon. Electrochem Solid State Lett **14**(2), G9–G12 (2011)
20. Pan, T.M., et al.: A urea biosensor based on pH-sensitive Sm2TiO5 electrolyte-insulator-semiconductor. Anal. Chim. Acta **669**(1–2), 68–74 (2010)
21. Shepelev, Y.F., Petrova, M.A.: Crystal structures of Ln(2)TiO(5) (Ln = Gd, Dy) polymorphs. Inorg. Mater. **44**(12), 1354–1361 (2008)
22. Lau, G.C., et al.: Stuffed rare earth pyrochlore solid solutions. J. Solid State Chem. **179**(10), 3126–3135 (2006)
23. Aughterson, R.D., et al.: The ion-irradiation tolerance of the pyrochlore to fluorite Ho(x)Yb(2–x)TiO5 and Er2TiO5 compounds: a TEM comparative study using both in-situ and bulk ex-situ irradiation approaches. J. Nucl. Mater. **507**, 316–326 (2018)
24. Aughterson, R.D., et al.: The crystal structures and corresponding ion-irradiation response for the Tb(x)Yb(2–x)TiO5 series. Ceram. Int. **44**(1), 511–519 (2018)
25. Lau, G.C., et al.: Long- and short-range order in stuffed titanate pyrochlores. J. Solid State Chem. **181**(1), 45–50 (2008)
26. Withers, R., Thompson, J., Barlow, P.: An electron, and X-ray powder, diffraction study of cubic, fluorite-related phases in various ZrO2 Ln2O3 systems. J. Solid State Chem. **94**(1), 89–105 (1991)
27. Tabira, Y., et al: The strain-driven pyrochlore to "defect fluorite" phase transition in rare earth sesquioxide stabilized cubic zirconias. **159**(1), 121–129 (2001)

28. Kennedy, B.J., Hunter, B.A., Howard, C.J.J.J.o.S.S.C: Structural and bonding trends in tin pyrochlore oxides. **130**(1), 58–65 (1997)
29. Newman, R., Aughterson, R.D., Lumpkin, G.R.: Synthesis and Structure of Novel A2BO5 Compounds Containing A = Y, Yb, Gd, Sm, and La and B = Zr, Ti, and Sn. MRS Advances **3**(20), 1117–1122 (2018)
30. Lian, J., et al: Radiation-induced amorphization of rare-earth titanate pyrochlores. Phys. Rev. B. **68**(13), 134107 (2003)
31. Park, S., et al.: Swift-heavy ion irradiation response and annealing behavior of A2TiO5 (A= Nd, Gd, and Yb). J. Solid State Chem. **258**, 108–116 (2018)
32. Shamblin, J., et al.: Structural response of titanate pyrochlores to swift heavy ion irradiation. Acta Mater. **117**, 207–215 (2016)
33. Wang, S.X., et al.: Radiation stability of gadolinium zirconate: a waste form for plutonium disposition. J. Mater. Res. **14**(12), 4470–4473 (1999)
34. Begg, B., et al.: Heavy-ion irradiation effects in Gd2 (Ti2− xZrx) O7 pyrochlores. J. Nucl. Mater. **289**(1–2), 188–193 (2001)
35. Lian, J., et al.: Ion-beam irradiation of Gd2Sn2O7 and Gd2Hf2O7 pyrochlore: Bond-type effect. J. Mater. Res. **19**(5), 1575–1580 (2004)
36. Lian, J., et al.: Ion beam irradiation in La2Zr2O7–Ce2Zr2O7 pyrochlore. Nucl. Instrum. Methods Phys. Res., Sect. B **218**, 236–243 (2004)
37. Cliff, G., Lorimer, G.W.: The quantitative analysis of thin specimens. J. Microsc. **103**(2), 203–207 (1975)
38. Hunter, B: Rietica - A Visual Rietveld Program. International Union of Crystallography Commission on Powder Diffraction. **Newsletter number 20 (Summer)** (1998)
39. Fink, D., et al.: The ANTARES AMS facility at ANSTO. Nucl. Instrum. Methods Phys. Res., Sect. B **223–224**, 109–115 (2004)
40. Ziegler, J. F., Ziegler, J.P.B., M. D., SRIM The Stopping and Range of Ions in Matter. www.SRIM.org (2008)
41. Lumpkin, G.R., et al.: Ion irradiation of ternary pyrochlore oxides. Chem. Mater. **21**(13), 2746–2754 (2009)
42. Stoller, R.E., et al.: On the use of SRIM for computing radiation damage exposure. Nucl. Instrum. Methods Phys. Res., Sect. B **310**, 75–80 (2013)
43. Aughterson, R.D., et al.: Crystal structures of orthorhombic, hexagonal, and cubic compounds of the Sm(x)Yb(2–x)TiO5 series. J. Solid State Chem. **213**, 182–192 (2014)
44. Rouanet, A.: Zirconium dioxide—Lanthanide oxide systems close to the melting point. Rev. Int. Hautes Temp. Refract **8**(2), 161–180 (1971)
45. Shannon, R.D.: Revised effective ionic radii and systematic studies of interatomic distances in halides and chalcogenides. Acta Crystallogr. A **32**, 751–767 (1976)
46. Mitchell, M.R., et al: 119 Sn MAS NMR and first-principles calculations for the investigation of disorder in stannate pyrochlores. **13**(2), 488–497 (2011)
47. de los Reyes, M., et al: The pyrochlore to defect fluorite phase transition in Y 2 Sn 2− x Zr x O 7. RSC Advances. **3**(15), 5090–5099 (2013)
48. Le Bail, A.: Whole powder pattern decomposition methods and applications: A retrospection. Powder Diffr. **20**(4), 316–326 (2005)
49. Whittle, K.R., et al.: Lanthanum pyrochlores and the effect of yttrium addition in the systems La2−xYxZr2O7 and La2−xYxHf2O7. J. Solid State Chem. **182**(3), 442–450 (2009)
50. Degen, T., et al: The highscore suite. **29**(S2), S13-S18 (2014)
51. Lian, J., et al.: Effect of structure and thermodynamic stability on the response of lanthanide stannate-pyrochlores to ion beam irradiation. J. Phys. Chem. B **110**(5), 2343–2350 (2006)
52. Tracy, C.L., et al: Role of composition, bond covalency, and short-range order in the disordering of stannate pyrochlores by swift heavy ion irradiation. Phys. Rev. B. **94**(6), 064102 (2016)
53. Sickafus, K.E., et al.: Radiation tolerance of complex oxides. Science **289**(5480), 748–751 (2000)
54. Naguib, H., Kelly, R.: Criteria for bombardment-induced structural changes in non-metallic solids. Radiat. Eff. **25**(1), 1–12 (1975)
55. Trachenko, K.: Understanding resistance to amorphization by radiation damage. J. Phys. Condensed Matt **16**(49), R1491–R1515 (2004)
56. Wang, S.X., et al.: Ion irradiation of rare-earth- and yttrium-titanate-pyrochlores. Nucl. Instrum. Methods. Phys. Res. Sect. B-Beam Interact. Mat. Atoms **169**, 135–140 (2000)
57. Lumpkin, G., et al: Radiation Tolerance of A2Ti2O7 Compounds at the Cubicmonoclinic Boundary, in Pacific Basin Nuclear Conference (15th : 2006 : Sydney, Australia). 2006, Australian Nuclear Association: Sydney, N.S.W. p. [703]-[709]